Acta Astronautica 179 (2021) 69–77

Contents lists available at ScienceDirect

Acta Astronautica

journal homepage: www.elsevier.com/locate/actaastro

Analytical guidance for circular orbit transfers with staging of space propulsion systems

Oliver Jia-Richards *, Paulo C. Lozano

Massachusetts Institute of Technology, Cambridge, MA, 02139, USA

ARTICLE INFO

Keywords:
Small spacecraft
Electrospray propulsion
Stage-based propulsion
Analytical
Guidance

ABSTRACT

This paper considers the combination of an analytical reference trajectory with linear state feedback control to allow for autonomous guidance and control of a spacecraft for coplanar circle-to-circle transfers with a stage-based propulsion system. Staging of electric propulsion components, such as tanks and thrusters, could allow small spacecraft to achieve high-ΔV capabilities with current propulsion technology. In order to utilize these propulsion systems, further developments in guidance and control of such spacecraft are required due to limitations in computational power and communications. Analytical approximations for low-thrust trajectories could allow for computationally simple guidance and control of autonomous spacecraft for circle-to-circle transfers around large central bodies. Many trajectories have been developed for conventional propulsion systems, based either on their shape or input thrust, and applied for preliminary mission design. A previously developed analytical trajectory is extended to account for the effects of staging propulsion system components. In order to stabilize the trajectory in the presence of disturbances, a linear state feedback control law is designed with linear quadratic regulator methods. Finally, a methodology for determining the correct phasing between the spacecraft and a target object is developed and is practical to implement on power-limited computers. The use of the analytical reference trajectory is simulated on an orbit transfer from low-Earth orbit to geostationary orbit.

1. Introduction

Small spacecraft with mass of 50 kg or lower, such as CubeSats, have demonstrated considerable capabilities for missions in low-Earth orbit [1]. However, their mission profiles have been limited by the availability of high-performance propulsion systems compatible with the small form factor. Due to difficulties with the miniaturization of propulsion systems, very few CubeSat propulsion systems have flight heritage, and the majority of those that do are cold-gas systems [2] which cannot be used for high-ΔV missions due to their low (~80 s) specific impulse. Since small spacecraft are typically launched as secondary payloads, the lack of high-performance propulsion systems means that their operational orbits are limited to the orbit of the primary payload, which places a significant restriction on the use of small spacecraft for missions beyond low-Earth orbit as rideshare opportunities are infrequent. To date, the only CubeSats to leave low-Earth orbit are the Mars Cube One spacecraft which were a secondary payload on the InSight mission to Mars.

The ability to raise and lower orbits will increase the capabilities and potential missions of small spacecraft. Such spacecraft can then continue to be launched as secondary payloads without restricting their final operating orbit. However, to enable this capability, high-ΔV propulsion systems compatible with the small form factor need to be developed. Furthermore, cost and user time limitations on communications between the spacecraft and Earth necessitate the development of autonomous guidance and control techniques. The use of staging of propulsion system components, analogous to launch vehicle staging, with microfabricated electrospray thrusters could deliver high-ΔV propulsion with currently available technology. Analytical approximations for low-thrust trajectories would enable autonomous guidance within the limits of computational power and memory available on small spacecraft, but cannot capture complex dynamics such as disturbances from other planets and solar radiation pressure. In order to stabilize the spacecraft trajectory to the analytical solution in the presence of disturbances, linear state feedback control could be used.

This work considers the combination of an analytical reference trajectory and linear feedback controller for circle-to-circle coplanar orbit transfers with a propulsion system comprised of a number of stages.

* Corresponding author.
E-mail address: oliverjr@mit.edu (O. Jia-Richards).

https://doi.org/10.1016/j.actaastro.2020.10.034
Received 20 December 2019; Received in revised form 14 October 2020; Accepted 15 October 2020
Available online 21 October 2020

Analytical expressions for the spacecraft's state and feedforward control as a function of time are developed by extending a derivation presented by Wiesel [3] to account for the effects of staging. Linear quadratic regulator methods are used to design a linear feedback controller in order to stabilize the trajectory and overcome the discrepancy in boundary conditions. Next, a methodology for determining the required phasing between the spacecraft and a rendezvous target is developed that is practical to implement on power-limited computers. Finally, the reference trajectory and linear controller are simulated for an orbit transfer from low-Earth orbit to geostationary orbit.

2. Background

The methodologies developed in this work are applicable to any propulsion system in either a conventional or staging configuration. However, staging with electrospray propulsion is a promising strategy in order to develop a high-ΔV propulsion systems compatible with small spacecraft, CubeSats included. This section provides background on electrospray thrusters as well as staging systems in order to enable miniaturized high-ΔV propulsion systems. An overview of analytical techniques for low-thrust orbit transfers is also provided, along with limitations of these techniques for use on an autonomous spacecraft using staged propulsion systems.

2.1. Electrospray propulsion

Electrospray thrusters produce thrust through electrostatic acceleration of either positively or negatively charged particles. A specific class of electrospray thruster is the ionic-liquid ion source where the charged particles are individual ions evaporated from an ionic liquid propellant [4] by overcoming the internal surface tension with a strong electric field [5]. The ionic liquid propellant is a molten salt at room temperature that is non-reactive, readily available, and has low toxicity. Electrospray thrusters with ionic liquid propellants hold three main advantages that make them ideal for main propulsion of small spacecraft. First, the ionic liquid is "pre-ionized" and does not need an ionization chamber. Second, ionic liquids have near-zero vapor pressure [6,7] and therefore do not need any form of pressurized containment and can be exposed directly to the vacuum of space. Lastly, propellant is fed to the thrusters by passive, capillary forces through a porous liner embedded into the fuel tank, thereby eliminating the need for bulky propellant management systems [8].

Several electrospray thruster designs based on microfabrication techniques have been proposed [9–12]. However, the ΔV output of current electrospray thrusters is limited by their operational lifetime. Difficulties with consistent manufacturing and inherent material non-uniformity [13,14] can lead to relatively wide emission cones with observed half angles of up to 60° [12]. The beam can therefore impact the extractor grid and allow propellant to accumulate on the extractor grid or backspray onto the emitter array. If enough propellant accumulates, an ionic liquid connection can form between the emitter array and extractor grid, causing an electrical short on the thruster and rendering it inoperable [11]. In addition, some emitter tips might have unstable menisci [15] which can lead to erratic liquid emission and occasional electrical discharges between the emitter tip and extractor grid [16] degrading the thruster over time.

The lifetime limitations, and therefore ΔV limitations, prevent the use of current electrospray thrusters for high-ΔV propulsion of small spacecraft. For example, the Ion Electrospray Propulsion System (IEPS) [12], shown in Fig. 1, has a demonstrated lifetime of approximately 500 h. On a 3U, 4 kg CubeSat, 32 thrusters can be placed on one of the 10 cm × 10 cm faces in order to produce 0.64 mN of thrust with a specific impulse of approximately 1000 s. The total ΔV capability of the propulsion system is therefore 292 m/s, enough ΔV to perform a low-thrust orbit raising around Earth from an orbital radius of 7000 km to 7575 km. This may be sufficient for some missions. However, missions that wish to go further to geostationary orbit, the Moon, or even deep space need significantly greater ΔV capabilities.

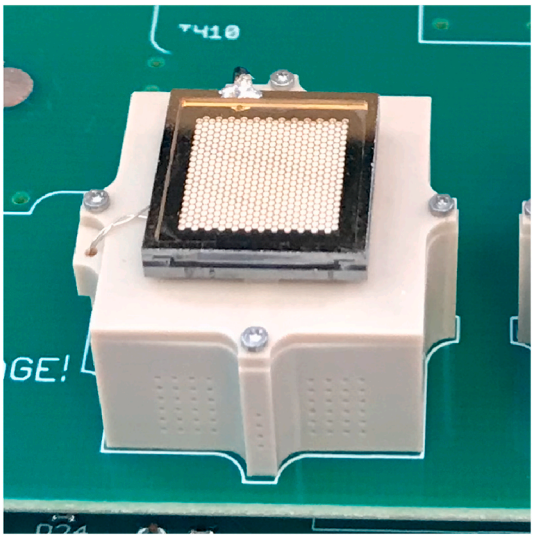

Fig. 1. IEPS thruster mounted on a single-thruster fuel tank.

2.2. Staging

To bypass the lifetime limitations of electrospray thrusters and improve their ΔV capabilities, two strategies could be taken: improve the lifetime of individual thrusters through a better understanding and mitigation of the life-limiting mechanisms, or bypass the lifetime limitations of individual thrusters through the use of staging. While the former strategy is continuously being explored and likely will bring lifetime improvements in the future, the latter presents itself as a strategy that could enable high-ΔV capabilities with existing electrospray technology. Furthermore, the use of staging systems in interplanetary missions would provide additional redundancy and reliability, even for thrusters with improved lifetime, as sets of fresh units could replace degraded ones. Efficient staging of electrospray thrusters is possible due to their small mass and volume, a unique feature not shared by other types of electric propulsion systems.

In a staged configuration, the propulsion system consists of a series of electrospray thruster arrays, each with their own set of fuel tanks. As each array reaches its lifetime limit, it is ejected from the spacecraft. This exposes a new array of thrusters that can then continue the mission. Fig. 2 shows a conceptual image of an electrospray thruster staging

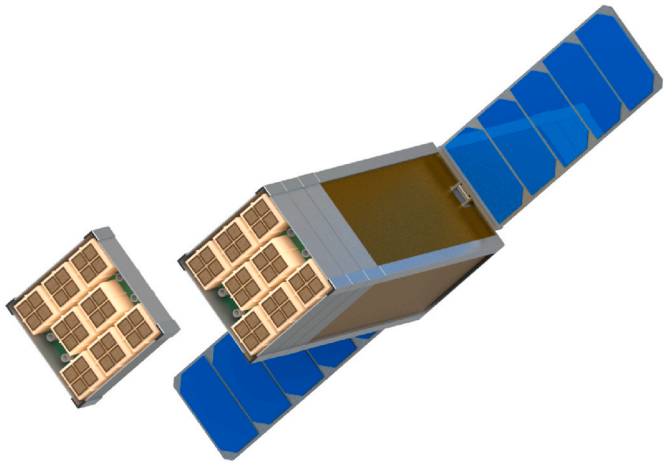

Fig. 2. Conceptual image of staging on a 3U CubeSat.

system on a 3U CubeSat. Staging was originally analyzed in order to reduce the overall transfer time from geostationary orbit to the Moon [17]. Since the spacecraft drops off structural mass at each staging event, the acceleration of each stage is increased relative to a single-stage system. Therefore, mission times can be reduced by a factor of around 10%. Staging with electrospray thrusters was further analyzed in Ref. [18] for enabling deep-space exploration with CubeSats where the spacecraft independently propels itself from Earth orbit and out into deep space. A laboratory demonstration of an electrospray-thruster-based staging system was conducted in Ref. [19] in order to demonstrate the mechanical and electrical feasibility of such a configuration. On the theoretical side, Ref. [20] analyzes the performance of staging systems including the overall reduction in mission time relative to a single-stage system and is consistent with the 10% factor seen in Ref. [17]. It is clear from Ref. [17,18,20] that the use of a stage-based system can significantly impact the spacecraft's trajectory and that trajectories designed under the assumption of a single-stage system will not be valid for a multi-stage one.

2.3. Analytical techniques for low-thrust orbit transfers

With the use of a stage-based electrospray propulsion system, high-ΔV propulsion (>3 km/s) for spacecraft as small as a CubeSat is possible with current technology. However, to actually perform these missions, guidance and control techniques amenable to the limited communication and computational power of such spacecraft need to be developed. In addition, these techniques need to be able to account for the effects of staging, specifically the discontinuity in spacecraft mass at each staging event.

Constraints on the computational power and memory available on CubeSats [21] limit the use of numerically propagated trajectories as these low-thrust trajectories can take several months to complete. Simple guidance schemes [22–24] have been developed specifically for this purpose and depend only on a few guidance parameters. However, these methods need to be tuned to a specific transfer scenario [22], and are therefore not robust to modeling errors, or control only the geometry of the orbit and not the actual spacecraft state [23,24].

The lack of robustness can pose problems for these long-duration transfers as accurate modeling of the propulsion system performance is difficult. The SMART-1 mission attempted to use an autonomous open-loop guidance scheme but saw unacceptable deviation of the spacecraft's trajectory after only a few days due to small errors in modeling the propulsion system's thrust output [25]. Controlling the orbit geometry can be useful for planning flyovers but prevents the use of the method for rendezvous.

Analytical reference trajectories could solve both of these issues. By providing an explicit reference trajectory, closed-loop feedback control can be used in order to stabilize the trajectory in the presence of disturbances. In addition, since the spacecraft trajectory is an algebraic function of time, such trajectories can be used for rendezvous. Analytical solutions to low-thrust trajectories have been developed since the early days of space flight [26–29] and a survey of many of the available solutions can be found in Ref. [30]. These analytical solutions have found use in preliminary mission design [31,32] but their consideration for use as reference trajectories has so far been unnecessary. The current paradigm of spacecraft operations for orbit-raising maneuvers on large spacecraft involves open-loop thrust durations with high-fidelity simulations of the spacecraft dynamics with on-Earth resources and frequent ground communications. In addition, the solutions in Ref. [30] have discrepancies in the boundary conditions between the analytical solution and spacecraft dynamics, meaning that they cannot be applied as an open-loop guidance scheme as is typically done. They also assume that any changes in spacecraft mass are due to fuel mass depletion and therefore cannot account for the effects of staging.

To the authors' knowledge, none of the available analytical low-thrust trajectories account for discontinuities in the spacecraft mass as would be seen with a staging system or have been tested as a reference trajectory for orbit transfers. Therefore, this work aims to extend one of the available analytical solutions [3] for use with a staging system and simulate its applicability as a reference trajectory for an orbit transfer. Although this method is developed with staging systems in mind, all results are applicable to a single-stage, conventional, system as a special case.

3. Analytical reference

The analytical trajectory used in this work is an extended version of an energy-based derivation presented by Wiesel [3]. This particular trajectory is selected as it assumes a constant propulsive acceleration which will be approximately true for low-thrust spirals. In addition, it assumes that the trajectory is quasi-circular which will ease stitching of different trajectory segments when accounting for staging and allow for the use of the Clohessy-Wiltshire frame in order to design a linear feedback controller. To correct the approximation and make the trajectory an exact solution of the spacecraft dynamics, the derivation is extended, in Section 3.1, by fixing the trajectory found from the initial derivation and then redefining the propulsive acceleration such that the spacecraft exactly follows the derived trajectory - similar to the shape-based derivations surveyed in Ref. [30]. The derivation is then extended again, in Section 3.2, to account for the effects of using a staging system. The resulting trajectory is then a piecewise function of time which is dynamically consistent except for the boundary conditions between intervals. The role of the trajectory controller in Section 4 is to correct for these discrepancies.

The specific energy of a spacecraft's orbit, ε, is given by

$$\varepsilon = \frac{1}{2}v^2 - \frac{\mu}{r} \tag{1}$$

where v is the velocity of the spacecraft, μ is the gravitational parameter of the central body, and r is the radial position of the spacecraft. Assuming that the orbit is circular, then the specific energy can be written as a function of only the orbital radius as

$$\varepsilon = -\frac{1}{2}\frac{\mu}{r} \tag{2}$$

The time derivative of the specific energy, the specific power, is therefore

$$\frac{d\varepsilon}{dt} = \frac{1}{2}\frac{\mu}{r^2}\frac{dr}{dt} \tag{3}$$

If the spacecraft carries a propulsion system that produces a constant propulsive acceleration a_p and assuming that the propulsive acceleration is aligned with the spacecraft's velocity, then the specific power input to the spacecraft's orbit from the propulsion system is

$$\frac{d\varepsilon}{dt} = a_p v = a_p\sqrt{\frac{\mu}{r}} \tag{4}$$

Assuming that the only power input to the spacecraft's orbit comes from its propulsion system, then we can equate Eqs. (3) and (4)

$$\frac{1}{2}\frac{\mu}{r^2}\frac{dr}{dt} = a_p\sqrt{\frac{\mu}{r}} \tag{5}$$

which can be rearranged to give an ordinary differential equation for the orbital radius

$$\frac{dr}{dt} = \frac{2a_p}{\sqrt{\mu}}r^{3/2} \tag{6}$$

This differential equation can be analytically integrated to give an approximation for the orbital radius as a function of time

$$r(t) = \frac{r_0}{\left(1 - \frac{a_p}{v_0} t\right)^2} \tag{7}$$

where r_0 is the initial orbital radius and v_0 is the initial orbital velocity. The radial velocity is simply the derivative of the orbital radius

$$v_r(t) = \frac{dr(t)}{dt} = \frac{2 r_0 a_p / v_0}{\left(1 - \frac{a_p}{v_0} t\right)^3} \tag{8}$$

The circumferential velocity can be approximated through the circular orbit approximation

$$v_\theta(t) = \sqrt{\frac{\mu}{r(t)}} = v_0 \left(1 - \frac{a_p}{v_0} t\right) \tag{9}$$

Lastly, the angular position can be approximated by integration

$$\theta(t) = \theta_0 + \int_0^t \frac{v_\theta(\tau)}{r(\tau)} d\tau = \theta_0 + \frac{1}{4} \frac{v_0^2}{r_0 a_p} \left[1 - \left(1 - \frac{a_p}{v_0} t\right)^4\right] \tag{10}$$

The trajectory given by this derivation is an approximation of the true spacecraft trajectory for a constant propulsive acceleration aligned with the velocity vector. The differences between the two trajectories are caused by the assumption that the spacecraft's orbit is always circular. While the error in the analytical trajectory will be small, especially for low-thrust trajectories, the lack of consistency between the analytical trajectory and spacecraft dynamics can cause problems for trajectory stabilization. In addition, the initial and final radial velocity for the analytical trajectory is not consistent with a circular orbit; the radial velocity given by Eq. (8) can not be zero unless the propulsive acceleration is also zero. This means that at the boundaries of the maneuver, the radial velocity given by the analytical trajectory will not match that of the desired initial and final circular orbits.

The problem with consistency between the reference trajectory and the spacecraft dynamics will be solved in the following section. However, the discrepancy in the initial and final radial velocity will persist. Therefore, a state feedback controller, discussed in Section 4, will be used to allow the spacecraft to join the trajectory from an initial circular orbit, and then leave the trajectory onto a final circular orbit.

3.1. Correction of control input

To correct for the inconsistency between the reference trajectory and the spacecraft's dynamics, the input acceleration is redefined. This process is similar to the shape-based approaches described in Refs. [30] where a desired trajectory is given and the propulsive acceleration is defined in order to allow the spacecraft to follow the trajectory.

Given the dynamics of the spacecraft's velocity

$$\dot{v}_r(t) = v_\theta^2(t) / r(t) - \mu / r^2(t) + a_r(t) \tag{12}$$

$$\dot{v}_\theta(t) = -v_r(t) v_\theta(t) / r(t) + a_\theta(t) \tag{13}$$

and the velocity derivatives of the trajectory from differentiating Eqs. (8) and (9)

$$\dot{v}_r(t) = \frac{6 r_0 a_p^2 / v_0^2}{\left(1 - \frac{a_p}{v_0} t\right)^4} \tag{14}$$

$$\dot{v}_\theta(t) = -a_p \tag{15}$$

the required a_r and a_θ to make the analytical trajectory consistent with the spacecraft's dynamics can be solved for

$$a_r(t) = \frac{6 r_0 a_p^2 / v_0^2}{\left(1 - \frac{a_p}{v_0} t\right)^4} \tag{16}$$

$$a_\theta(t) = a_p \tag{17}$$

The required propulsive acceleration is larger than the initial acceleration used to size the trajectory, a_p. However, for low-thrust trajectories, $a_p \ll v_0^2 / r_0$ which means that $a_r \approx 0$ unless $t \approx v_0 / a_p$. This will hold for circle-circle transfers around a large central body since from Eq. (7) as $t \to v_0 / a_p$ then $r \to \infty$ so the actual propulsive acceleration of the spacecraft can be used to size the trajectory with the slow increase in a_r being accounted for by the reduction in spacecraft mass due to fuel mass flow.

3.2. Extension to staging

Staging impacts the trajectory through discrete drops in the spacecraft's mass over time. While the trajectory in Eqs. (7)–(10) could continue to be followed by reducing the propulsion system's thrust, a trajectory that accounts for the increased available propulsive acceleration will be faster and more fuel efficient.

To account for the impact of staging, the trajectory is expressed as a piecewise function of time where each interval corresponds to an individual stage. The trajectory in each interval will be given by Eqs. (7)–(10)) and the initial radial position, r_0, and velocity, v_0, will need to be correctly defined in order to link the intervals together. Since all the state variables are defined based on the radial position, the impact of staging will first be analyzed by defining the radial position over each interval from which the other state variables will be derived.

Assuming that the propulsion system produces thrust F, the initial spacecraft wet mass is m_0, and that the propulsive acceleration is constant for each stage, then the radial position for the first stage, r_1, is given by

$$r_1(t_1) = \frac{r_0}{\left(1 - \frac{F}{v_0 m_0} t_1\right)^2} \tag{18}$$

where t_1 is the firing time for the first stage. If each stage has lifetime L then the radial position of the spacecraft at the end of the first stage's firing will be

$$r_1(L) = \frac{r_0}{\left(1 - \frac{F}{v_0 m_0} L\right)^2} \tag{19}$$

The second stage then continues the trajectory starting from $r_1(L)$. In addition, the mass of the spacecraft is reduced by the wet mass of the first stage, m_s. Therefore, the radial position of the spacecraft during second stage firing is given by

$$r_2(t_2) = \frac{r_1(L)}{\left(1 - \frac{F}{v_{0,2}(m_0 - m_s)} t_2\right)^2} \tag{20}$$

where the initial velocity, $v_{0,2}$ is given by

$$v_{0,2} = \sqrt{\frac{\mu}{r_1(L)}} = v_0 \left(1 - \frac{F}{v_0 m_0} L\right) \tag{21}$$

Substituting Eqs. (19) and (21) into Eq. (20) gives

$$r_2(t_2) = \frac{r_0}{\left(1 - \frac{F}{v_0 m_0} L - \frac{F}{v_0 (m_0 - m_s)} t_2\right)^2} \tag{22}$$

Continuing this argument to a third stage gives

$$r_3(t_3) = \frac{r_2(L)}{\left(1 - \frac{F}{v_{0,3}(m_0 - 2m_s)} t_3\right)^2} \tag{23}$$

where

$$r_2(L) = \frac{r_0}{\left(1 - \frac{F}{v_0 m_0} L - \frac{F}{v_0 (m_0 - m_s)} L\right)^2} \tag{24}$$

and

$$v_{0,3} = \sqrt{\frac{\mu}{r_2(L)}} = v_0 \left(1 - \frac{F}{v_0 m_0} L - \frac{F}{v_0 (m_0 - m_s)} L\right) \tag{25}$$

which results in

$$r_3(t_3) = \frac{r_0}{\left(1 - \frac{F}{v_0 m_0} L - \frac{F}{v_0 (m_0 - m_s)} L - \frac{F}{v_0 (m_0 - 2m_s)} t_3\right)^2} \tag{27}$$

In general, for any stage n, the radial position of the spacecraft is given by

$$r_n(t_n) = \frac{r_0}{\left(1 - \frac{\Delta V_{1:n-1}}{v_0} - \frac{F}{v_0 m_n} t_n\right)^2} \tag{28}$$

where

$$m_n = m_0 - (n-1) m_s \tag{29}$$

$$\Delta V_{1:n-1} = \begin{cases} 0 & n = 1 \\ \sum_{i=1}^{n-1} \frac{FL}{m_0 - (i-1) m_s} & n > 1 \end{cases} \tag{30}$$

the radial velocity is still given by the derivative of the radial position

$$v_{r,n}(t_n) = \frac{2 r_0 F / v_0 m_n}{\left(1 - \frac{\Delta V_{1:n-1}}{v_0} - \frac{F}{v_0 m_n} t_n\right)^3} \tag{31}$$

and the circumferential velocity is still approximated through the circular orbit approximation

$$v_{\theta,n}(t_n) = v_0 \left(1 - \frac{\Delta V_{1:n-1}}{v_0} - \frac{F}{v_0 m_n} t_n\right) \tag{32}$$

The angular position of the spacecraft requires extra work. The angular position during each interval is given by

$$\theta_n(t_n) = \theta_{0,n} + \int_0^{t_n} \frac{v_{\theta,n}(t)}{r_n(t)} dt = \theta_{0,n} + \int_0^{t_n} \frac{v_0}{r_0} \left(1 - \frac{\Delta V_{1:n-1}}{v_0} - \frac{F}{v_0 m_n} t\right)^3 dt \tag{33}$$

Carrying out the integration gives

$$\theta_n(t_n) = \theta_{0,n} + \frac{1}{4} \frac{v_0^2 m_n}{r_0 F} \left[\Gamma^4 - \left(\Gamma - \frac{F}{v_0 m_n} t_n\right)^4\right] \tag{35}$$

where

$$\Gamma = 1 - \frac{\Delta V_{1:n-1}}{v_0} \tag{36}$$

The initial angular position for each interval can then be defined recursively as

$$\theta_{0,n} = \begin{cases} \theta_0 & n = 1 \\ \theta_{n-1}(L) & n > 1 \end{cases} \tag{37}$$

Finally, in order to ensure that the reference trajectory is consistent with the spacecraft dynamics, Eqs. (16) and (17) are extended for each stage, n, which gives a control input during each interval of

$$a_{r,n}(t_n) = \frac{6 r_0 F^2 / v_0^2 m_n^2}{\left(1 - \frac{\Delta V_{1:n-1}}{v_0} - \frac{F}{v_0 m_n} t_n\right)^4} \tag{38}$$

$$a_{\theta,n}(t_n) = \frac{F}{m_n} \tag{39}$$

where $a_{r,n} = \dot{v}_{r,n}$ and $a_{\theta,n} = a_{p,n}$ which are both consequences of the circular orbit approximation.

3.3. Numerical comparison

The analytical reference is compared against a numerical simulation of a standard velocity-pointing control law. The trajectory of a spacecraft, with properties given by Table 1, is simulated from an initial 10,000 km circular orbit until the orbital radius of the spacecraft reaches 20,000 km. Along the trajectory, stages are dropped, causing the mass of the spacecraft to decrease as each stage reaches its lifetime limit. The stage mass in Table 1 accounts for both the structural mass of the stage as well as the mass of fuel used throughout the stage's lifetime assuming a specific impulse of approximately 1500 s.

Fig. 3 shows the error in radial position between the analytical reference in Eq. (28) relative to the numerical simulation for both the entire trajectory and around the second staging event. The normalized time, $\bar{t}$, is the trajectory time normalized by the stage lifetime such that $\bar{t} \in \{1, 2, 3, \ldots\}$ corresponds to staging events. The error in the analytical reference is oscillatory, centered around zero. This is due to the circular orbit assumption as the analytical reference does not capture the effect of eccentricity. However, it gives the average motion of the spacecraft.

Fig. 4 shows the radial velocity for both the numerical simulation and analytical references near the second staging event ($\bar{t} = 2$). Again, time is normalized by the stage lifetime. Immediately after the staging, the numerical simulation is continuous, but the center of the oscillations increases slightly. The analytical reference is discontinuous, but also increases such that the analytical reference tracks the center of the numerical trajectory.

The analytical reference gives the average motion of the spacecraft for all of the state variables in the orbital plane if the spacecraft were to use a velocity-pointing control law. For radial position, angular position, and circumferential velocity, the analytical reference is continuous and tracks the average change in each variable. However, for the radial velocity, the analytical reference is discontinuous at each staging event. This necessitates a state feedback controller that can correct for the discontinuity at the beginning of the trajectory, after each staging event, and at the end of the trajectory. If the discontinuities in radial velocity were corrected and the spacecraft used Eqs. (38) and (39) for its control law in each interval, then the analytical reference would exactly match the numerical simulation.

4. Trajectory control

The trajectory controller serves to correct the discontinuities in the radial velocity of the analytical reference and also to reject any disturbances throughout the trajectory. The controller considered in this work

Table 1
Spacecraft and propulsion system properties.

Property	Value
Initial mass	4 kg
Stage mass	0.2 kg
Thrust	0.64 mN
Stage lifetime	1000 h

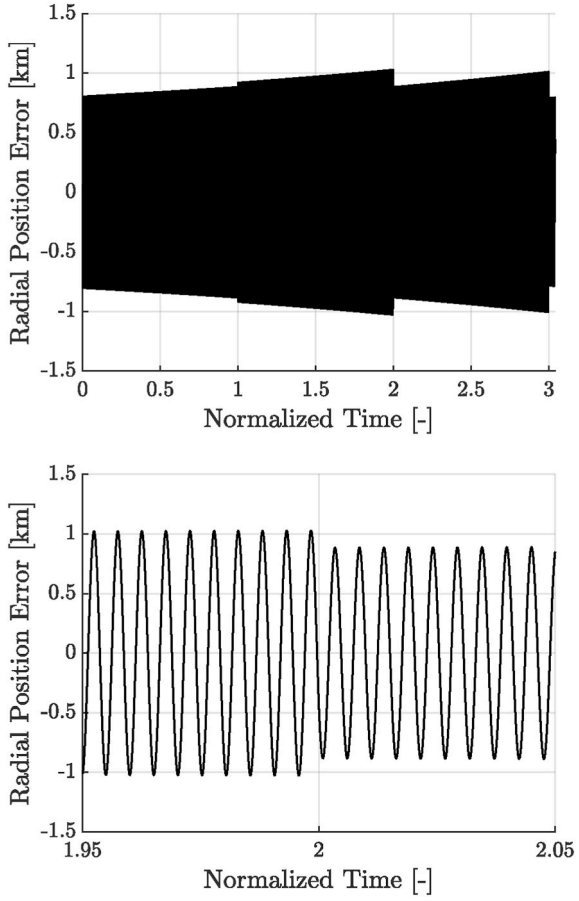

Fig. 3. Error in radial position between the analytical reference and a numerical simulation versus time normalized by the stage lifetime. Top plot shows the entire trajectory while the bottom plot shows the error around the second staging event.

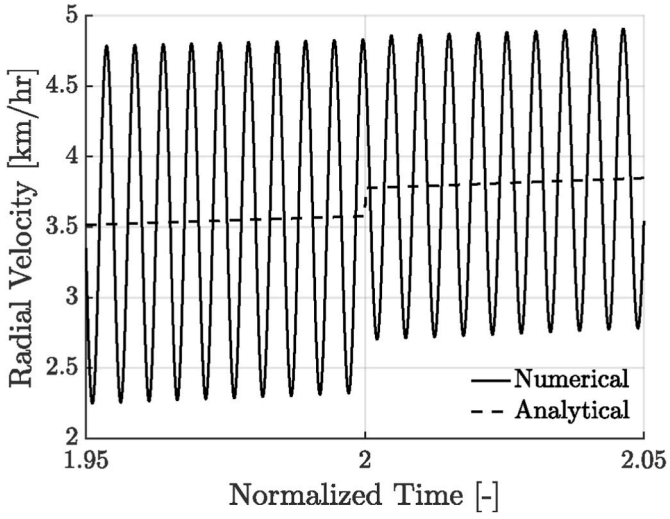

Fig. 4. Radial velocity of the numerical simulation and analytical reference versus time normalized by the stage lifetime around the second staging event.

is a continuous-time, linear feedback controller designed with linear quadratic regulator (LQR) methods in order to maintain computational simplicity. For the linearized dynamics model, the Clohessy-Wiltshire frame is used, as the spacecraft's trajectory is quasi-circular and the propulsive acceleration is small relative to the local gravitational acceleration. It is also assumed that the spacecraft is fully actuated and can produce thrust in any desired direction. Although attitude control will not be considered in this work, the use of electrospray thrusters for precise attitude control has been demonstrated previously in a laboratory environment [33].

The linear dynamics model used to determine the controller gains is therefore

$$\begin{bmatrix} \dot{x} \\ \dot{y} \\ \dot{v}_x \\ \dot{v}_y \end{bmatrix} = \begin{bmatrix} 0 & 0 & 1 & 0 \\ 0 & 0 & 0 & 1 \\ 3n^2 & 0 & 0 & 2n \\ 0 & 0 & -2n & 0 \end{bmatrix} \begin{bmatrix} x \\ y \\ v_x \\ v_y \end{bmatrix} + \begin{bmatrix} 0 & 0 \\ 0 & 0 \\ 1 & 0 \\ 0 & 1 \end{bmatrix} \begin{bmatrix} a_x \\ a_y \end{bmatrix} \tag{40}$$

where the xy frame is centered on the analytical reference trajectory, x points in the radial direction, and y is aligned with the circumferential velocity. n is the angular frequency of the quasi-circular orbit,

$$n = \sqrt{\mu / r^3} \tag{41}$$

a_x and a_y are control accelerations that are applied in addition to the accelerations given by Eqs. (38) and (39) in order to stabilize the spacecraft to the reference trajectory. Only the states and control accelerations in the orbital plane are considered here as the dynamics perpendicular to the orbital plane are decoupled from those in the orbital plane.

A linear feedback controller

$$u_{\mathrm{fb}} = -Ks_{\mathrm{e}} \tag{42}$$

is used where s_{e} and u_{fb} are the error in the spacecraft state relative to the reference trajectory and the feedback control accelerations in the Clohessy-Wiltshire frame respectively

$$s_e = \begin{bmatrix} x \\ y \\ v_x \\ v_y \end{bmatrix} \quad \text{and} \quad u_{\mathrm{fb}} = \begin{bmatrix} a_x \\ a_y \end{bmatrix} \tag{43}$$

and K is a matrix of control gains calculated in order to minimize the infinite horizon LQR cost function

$$J = \int_{t_0}^{\infty} \left[s_{\mathrm{e}}^T Q s_{\mathrm{e}} + u_{\mathrm{fb}}^T R u_{\mathrm{fb}} \right] dt \tag{44}$$

where Q and R are weighting matrices.

Since the dynamics matrices in Eq. (40) depend on the spacecraft radial position, the optimal control gains will also change with radial position. If the difference in initial and final radius is large, then the control gains can vary significantly throughout the trajectory. In order to account for this, the controller gains at a particular orbital radius, r, were calculated through linear interpolation as

$$K = K_0 + \left(K_f + K_0\right) \frac{r - r_0}{r_f - r_0} \tag{45}$$

where K_0 are the optimal gains at the initial orbital radius, r_0, and K_f are the optimal gains at the final orbital radius, r_f. The linear interpolation allows for smooth transitioning of the controller gains while avoiding the computational complexity of calculating the optimal gains at each orbital radius. In addition, the linear interpolation was found to produce comparable results to calculating the optimal gains at every orbital radius, with errors in the final state being dominated by any disturbances added to the simulation such as the gravitational force of the Moon.

5. Implementation

Throughout all tests, the required propulsive acceleration was calculated as

$$\begin{bmatrix} a_r(t) \\ a_\theta(t) \end{bmatrix} = \begin{bmatrix} a_{r,n}(t_n) \\ a_{\theta,n}(t_n) \end{bmatrix} - Ks_e \tag{46}$$

where $a_{r,n}(t_n)$ and $a_{\theta,n}(t_n)$ are calculated according to Eqs. (38) and (39) and the linear feedback controller is from Section 4, with gains given by Eq. (45) and weighting matrices set as

$$Q = \begin{bmatrix} 10 & 0 & 0 & 0 \\ 0 & 10 & 0 & 0 \\ 0 & 0 & 1 & 0 \\ 0 & 0 & 0 & 1 \end{bmatrix} \quad \text{and} \quad R = \begin{bmatrix} 1 & 0 \\ 0 & 1 \end{bmatrix} \tag{47}$$

The time for a given stage, t_n, is calculated as

$$t_n = t - (n-1)L \tag{48}$$

The spacecraft has properties given by Table 1 which are representative of an IEPS-based propulsion system on a 3U CubeSat. The thrust used to size the reference trajectory is 75% that of the thrust in Table 1. This is to allow for extra thrust to be applied in order to stabilize the trajectory without saturating the thrust of the propulsion system. The thrust output of the propulsion system with the feedback controller is therefore

$$\begin{bmatrix} F_r(t) \\ F_\theta(t) \end{bmatrix} = m_n \begin{bmatrix} a_r(t) \\ a_\theta(t) \end{bmatrix} \tag{49}$$

and is saturated such that

$$\sqrt{F_r^2(t) + F_\theta^2(t)} \leq F_{\max} \tag{50}$$

where $F_{\max}$ is the thrust given in Table 1.

The spacecraft follows the trajectory defined by Eqs. (28), (31), (32) and (35) from an initial orbital radius, r_0, to a final orbital radius, r_f. Once the spacecraft reaches r_f, it is provided with a circular reference trajectory in order to correct for the excess radial velocity in the transfer reference trajectory from evaluating Eq. (31) at the final time and stabilize the spacecraft to the desired final orbit.

If the reference trajectory is to be used for rendezvous, then the total angular position change of the spacecraft needs to be known in order to calculate the phasing between the spacecraft and the target. Assuming that the number of stages and total trajectory time are known, then the total angular position change of the spacecraft can be calculated from Eq. (35) with an assumed initial angular position at the beginning of the trajectory of zero ($\theta_0 = 0$). The number of stages and trajectory time can be solved based on the radial position. We know that at the end of each stage's interval, the radial position will be given by

$$r_n(L) = \frac{r_0}{\left(1 - \frac{1}{v_0}\sum_{i=1}^{n} \frac{FL}{m_0 - (i-1)m_s}\right)^2} \tag{51}$$

Therefore, the required number of stages in order to reach a final orbital radius of r_f can be found by determining the lowest n such that $r_n(L) \geq r_f$. This value can be calculated numerically or approximated analytically. The summation in the denominator of Eq. (51) is equal to the ΔV provided by n stages when a constant propulsive acceleration is used for each stage

$$\Delta V_n = \sum_{i=1}^{n} \frac{FL}{m_0 - (i-1)m_s} \tag{52}$$

One possible analytical approximation for this ΔV assumes that the total impulse of all n stages is applied to the time-average mass of the spacecraft

$$\Delta V_n \approx \frac{nFL}{m_0 - \frac{1}{2}(n-1)m_s} \tag{53}$$

and is shown to estimate the numerical calculation of the ΔV to within 5% [20]. Using the analytical approximation for ΔV_n and solving Eq. (51) for the approximate number of stages in the case that $r_n(L) = r_f$ gives

$$n \approx \frac{\left(m_0 + \frac{1}{2}m_s\right)\left(1 - \sqrt{r_0/r_f}\right)}{FL \Big/ v_0 + \frac{1}{2}m_s\left(1 - \sqrt{r_0/r_f}\right)} \tag{54}$$

The approximation for number of stages permits non-integer values. In this case, the last stage is only used to some fraction of its lifetime. The actual, integer, number of stages is found by rounding the output of Eq. (54) up to the next highest integer.

With the number of required stages calculated numerically or approximated analytically, the radial position of the spacecraft on the last stage is given by Eq. (28). The stage time, $t_{n,f}$, at which the spacecraft reaches the final orbital radius, r_f, can then be calculated by solving Eq. (28) for t_n in the case that $r_n(t_n) = r_f$. This gives

$$t_{n,f} = \frac{v_0 m_n}{F}\left(\sqrt{\frac{r_0}{r_f}} + \frac{\Delta V_{1:n-1}}{v_0} - 1\right) \tag{55}$$

The total angular change of the spacecraft, $\Delta\theta_{1:n}$, can then be calculated from Eq. (35) with $t_n = t_{n,f}$. The total angular change of the target, $\Delta\theta_t$, throughout the spacecraft's trajectory is given by

$$\Delta\theta_t = \left[t_{n,f} + (n-1)L\right]\sqrt{\frac{\mu}{r_f^3}}$$

which allows the initial phasing between the spacecraft and the target, φ, to be calculated as

$$\varphi = \Delta\theta_{1:n} - \Delta\theta_t \tag{56}$$

Using either a numerical calculation or analytical approximation of the required number of stages, Eq. (56) can be calculated through a chain of algebraic operations. This means that calculating the required phasing is practical for implementation on small spacecraft where computational power is limited, which could enable autonomous rendezvous.

6. Results

For demonstration, the analytical reference trajectory and linear state feedback control law are tested on a orbit transfer from low-Earth orbit (7000 km) to geostationary orbit (42,164 km) with implementation details described in Section 5. Fig. 5 shows the radial position of the spacecraft during the orbit transfer versus time normalized by the stage lifetime. Eq. (54) predicted 8.43 stages required for the transfer and the spacecraft reached the final orbital radius in 8.28 stages (1.8% error).

Fig. 6 shows the angular position error relative to the reference trajectory during the orbit transfer versus time normalized by the stage lifetime. Due to the initial discrepancy in the radial velocity, the spacecraft is initially in a lower orbit than the reference trajectory and as such, the angular position of the spacecraft moves ahead of the reference trajectory. The error the spacecraft obtains (~0.005°) remains constant throughout the transfer trajectory. Once the spacecraft completes the transfer, it overshoots the final orbital radius due to the non-zero radial velocity in the reference trajectory. This causes the spacecraft's angular position to drift behind the reference. The resulting negative error in angular position slowly gets corrected over time as the spacecraft regulates itself to the final orbit.

Fig. 7 shows the error in the radial velocity of the spacecraft relative to the reference trajectory during the orbit transfer versus time normalized by the stage lifetime. At each staging event (integer values of time), the error in the radial velocity spikes due to the discontinuity from

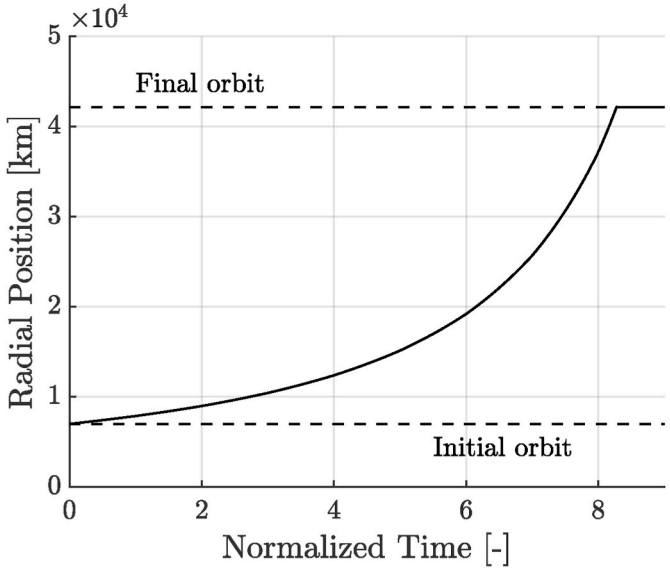

Fig. 5. Radial position of the spacecraft during the orbit transfer versus time normalized by the stage lifetime.

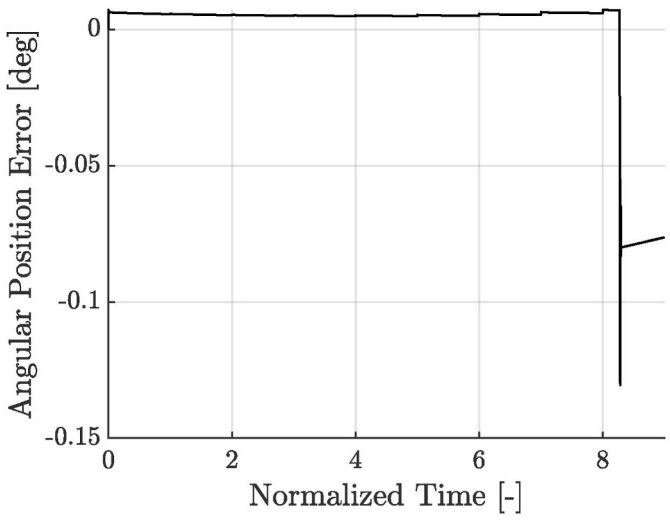

Fig. 6. Error in angular position of the spacecraft relative to the reference trajectory during the orbit transfer versus time normalized by the stage lifetime.

Eq. (31). However, the magnitude of the discontinuity is small (<0.1 m/s) and the state feedback controller is able to stabilize the trajectory. Another discontinuity occurs at the end of the transfer trajectory once the spacecraft reaches its final orbital radius. However, this discontinuity is also small (~5 m/s) and the feedback controller is again able to correct for it.

Based on Eq. (56), the required phasing between the spacecraft and a potential rendezvous target is 135.4°, meaning that the spacecraft needs to start 135.4° behind the target. Fig. 8 shows the distance between the spacecraft and rendezvous target during the orbit transfer versus time normalized by the stage lifetime. Initially the distance oscillates between roughly 35,000 km and 49,000 km, which is expected since the spacecraft is in a 7000 km orbit and the target is in a 42,164 km orbit. The oscillations continue to grow, until on the last leg of the transfer trajectory the spacecraft-target distance falls to near zero. The distance between the spacecraft and target at the end of the simulation is approximately 56 km and is primarily driven by the error in angular position. However, as seen in Fig. 6, the angular position error is slowly decreasing at the end of the simulation and over time the spacecraft-target distance will approach zero.

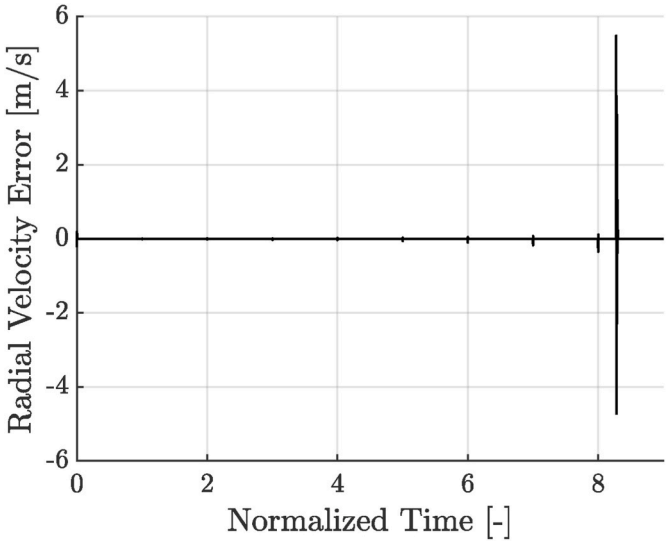

Fig. 7. Error in radial velocity of the spacecraft relative to the reference trajectory during the orbit transfer versus time normalized by the stage lifetime.

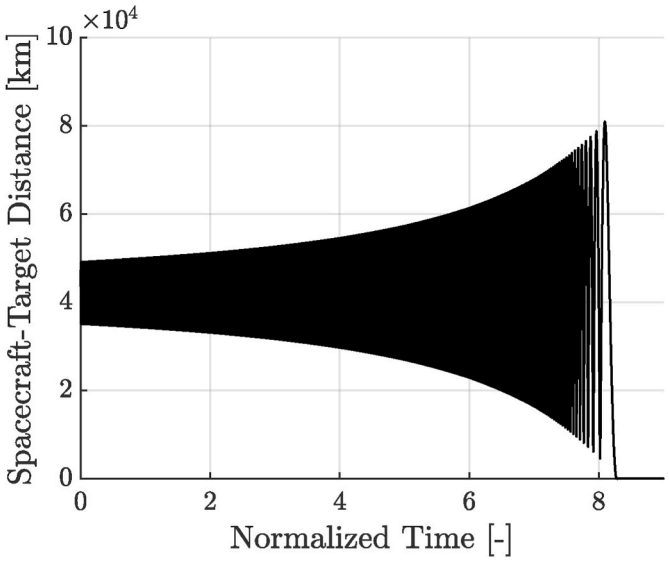

Fig. 8. Distance between the spacecraft and rendezvous target during the orbit transfer versus time normalized by the stage lifetime.

7. Conclusion

An analytical reference trajectory with linear state feedback controller is shown in simulation to be able to guide a spacecraft with a stage-based propulsion system between two circular coplanar orbits, with application to autonomous rendezvous. A previously derived analytical approximation for low-thrust spirals is extended to make the trajectory consistent with the spacecraft dynamics and to account for the effects of staging. The resulting trajectory is piecewise in time with each interval corresponding to an individual stage. The required phasing between a spacecraft and rendezvous target can be solved for algebraically, allowing for practical implementation on power-limited computers.

Use of the analytical reference for rendezvous is simulated for a spacecraft starting in low-Earth orbit and rendezvousing with a target in geostationary orbit. The final distance between the spacecraft and target

at the end of simulation is 56 km, but is slowly decreasing over time. The final distance is driven by error in the spacecraft's angular position, which is a byproduct of the discontinuity in radial velocity when joining and leaving the reference trajectory. However, the spacecraft-target distance is small enough that alternative guidance methods can take over for proximity operations.

Analytical reference trajectories with linear state feedback controllers could allow for computationally simple guidance and control of autonomous spacecraft during orbit transfers and rendezvous. While not as accurate as numerically propagated trajectories, the use of a propulsion system with a continuous range of thrust levels, such as electrospray thrusters, can be used to correct for the external disturbances and allow for the use of the simplified trajectory. The combination of a stage-based electrospray propulsion system, to enable high-ΔV propulsion for small spacecraft, and analytical reference, for computationally simple guidance, could dramatically increase the capabilities of small spacecraft.

Declaration of competing interest

The authors declare that they have no known competing financial interests or personal relationships that could have appeared to influence the work reported in this paper.

Acknowledgements

Funding for this work was provided by the NASA Space Technology Mission Directorate through a NASA Space Technology Research Fellowship under grant 80NSSC18K1186 and through the Small Spacecraft Technology Program under grant 80NSSC18M0045. In addition, PCL would like to thank the Miguel Alemán-Velasco Foundation for its support.

References

[1] D. Selva, D. Krejci, A survey and assessment of the capabilities of CubeSats for earth observation, Acta Astronaut. 74 (2012) 50–68, https://doi.org/10.1016/j.actaastro.2011.12.014.
[2] K. Lemmer, Propulsion for CubeSats, Acta Astronaut. 134 (2017) 231–243, https://doi.org/10.1016/j.actaastro.2017.01.048.
[3] W.E. Wiesel, Spaceflight Dynamics, second ed., McGraw-Hill, New York, 1997, pp. 90–92.
[4] S.A. Forsyth, J.M. Pringle, D.R. MacFarlane, Ionic liquidsâ€"an overview, Aust. J. Chem. 57 (2) (2004) 113–119, https://doi.org/10.1071/CH03231.
[5] P. Lozano, M. Martinez-Sanchez, Ionic liquid ion sources: characterization of externally wetted emitters, J. Colloid Interface Sci. 282 (2) (2005) 415–421, https://doi.org/10.1016/j.jcis.2004.08.132.
[6] L.P.N. Rebelo, J.N. Canongia Lopes, J.M.S.S. Esperanca, E. Filipe, On the critical temperature, normal boiling point, and vapor pressure of ionic liquids, J. Phys. Chem. B 109 (13) (2005) 6040–6043, https://doi.org/10.1021/jp050430h.
[7] M.J. Earle, J.M.S.S. Esperanca, M.A. Gilea, J.N. Canongia Lopes, L.P.N. Rebelo, J. W. Magee, K.R. Seddon, J.A. Widegren, The distillation and volatility of ionic liquids, Nature 439 (7078) (2006) 831–834, https://doi.org/10.1038/nature04451.
[8] D.G. Courtney, H.Q. Li, P. Lozano, Emission measurements from planar arrays of porous ionic liquid ion sources, J. Phys. Appl. Phys. 45 (48) (2012) 485203, https://doi.org/10.1088/0022-3727/45/48/485203.
[9] M.S. Alexander, J. Stark, K.L. Smith, B. Stevens, B. Kent, Electrospray performance of microfabricated colloid thruster arrays, J. Propul. Power 22 (3) (2006) 620–627, https://doi.org/10.2514/1.15190.
[10] R.S. Legge, P.C. Lozano, Electrospray propulsion based on emitters microfabricated in porous metals, J. Propul. Power 27 (2) (2011) 485–495, https://doi.org/10.2514/1.50037.
[11] E. Grustan-Gutierrez, M. Gamero-Castano, Microfabricated electrospray thruster array with high hydraulic resistance channels, J. Propul. Power 33 (4) (2017) 984–991, https://doi.org/10.2514/1.B36268.
[12] D. Krejci, F. Mier-Hicks, R. Thomas, T. Haag, P.C. Lozano, Emission characteristics of passively fed electrospray microthrusters with propellant reservoirs, J. Spacecraft Rockets 54 (2) (2017) 447–458, https://doi.org/10.2514/1.A33531.
[13] J. Rojas-Herrera, C. Fucetola, D. Krejci, D. Freeman, I. Jivanescu, P. C. Lozano, Porous materials for ion-electrospray spacecraft micro-engines, Nanomechanics and Micromechanics 7 (3). doi:10.1061/(ASCE)NM.2153-5477.0000121.
[14] J. Rojas-Herrera, P.C. Lozano, Mitigation of anomalous expansion of carbon xerogels and controllability of mean-pore-size by changes in mold geometry, J. Non-Cryst. Solids 458 (2017) 22–27, https://doi.org/10.1016/j.jnoncrysol.2016.12.015.
[15] F. J. H. Chase Coffman, Manuel Martinez-Sanches, P. C. Lozano, Structure of the menisci of leaky dielectric liquids during electrically-assisted evaporation of ions, Appl. Phys. Lett. 109 (23). doi:10.1063/1.4971778.
[16] N. Brikner, P. C. Lozano, The role of upstream distal electrodes in mitigating electrochemical degradation of ionic liquid ion sources, Appl. Phys. Lett. 101 (19). doi:10.1063/1.4766293.
[17] D. Krejci, M.G. Jenkins, P.C. Lozano, Staging of electric propulsion systems: enabling an interplanetary CubeSat, Acta Astronaut. 160 (2019) 175–182, https://doi.org/10.1016/j.actaastro.2019.04.031.
[18] O. Jia-Richards, P.C. Lozano, Stage-based electrospray propulsion system for deep-space exploration with CubeSats, in: Proceedings of the 40th IEEE Aerospace Conference, Big Sky, MT, 2019, https://doi.org/10.1109/AERO.2019.8742094.
[19] O. Jia-Richards, P.C. Lozano, Laboratory demonstration of a staging system for electrospray thrusters, in: Proceedings of the 36th International Electric Propulsion Conference, 2019. Vienna, Austria.
[20] O. Jia-Richards, P.C. Lozano, An analytical framework for staging of space propulsion systems, J. Propul. Power 36 (4) (2020) 527–534, https://doi.org/10.2514/1.B37722.
[21] J. Schoolcraft, A.T. Klesh, T. Werne, MarCO, Interplanetary Mission Development on a CubeSat Scale, *14th International Conference on Space Operations*, 2016, https://doi.org/10.2514/6.2016-2491. Daejeon, Korea.
[22] C.A. Kluever, Simple guidance scheme for low-thrust orbit transfers, J. Guid. Contr. Dynam. 21 (6) (1998) 1015–1017, https://doi.org/10.2514/2.4344.
[23] M. Guelman, Closed-loop control of close orbits around asteroids, J. Guid. Contr. Dynam. 38 (5) (2014) 854–860, https://doi.org/10.2514/1.G000158.
[24] M.M. Guelman, A. Shiryaev, Closed-loop control of earth observation satellites, J. Spacecraft Rockets 56 (1) (2018) 82–90, https://doi.org/10.2514/1.A34134.
[25] P. Rathsman, J. Kugelberg, P. Bodin, G.D. Racca, B. Foing, L. Stagnaro, SMART-1: development and lessons learnt, Acta Astronaut. 57 (2) (2005) 455–468, https://doi.org/10.1016/j.actaastro.2005.03.041.
[26] H.S. Tsien, Take-off from satellite orbit, J. Am. Rocket Soc. 23 (4) (1953) 233–236, https://doi.org/10.2514/8.4599.
[27] T.C. Tsu, Interplanetary travel by solar sail, ARS J. 29 (6) (1959) 422–427, https://doi.org/10.2514/8.4791.
[28] T.N. Edelbaum, Propulsion requirements for controllable satellites, ARS J. 31 (8) (1961) 1079–1089, https://doi.org/10.2514/8.5723.
[29] W.E. Wiesel, S. Alfano, Optimal many-revolution orbit transfer, J. Guid. Contr. Dynam. 8 (1) (1985) 155–157, https://doi.org/10.2514/3.19952.
[30] A.E. Petropoulos, J.A. Sims, A review of some exact solutions to the planar equations of motion of a thrusting spacecraft, in: Proceedings of the 2nd International Symposium of Low Thrust Trajectores, France, Toulouse, 2002.
[31] M. Macdonald, Analytical, circle-to-circle low-thrust transfer trajectories with plane change, in: Proceedings of AIAA Guidance, Navigation, and Control Conference, 2013, https://doi.org/10.2514/6.2013-5026. Boston, MA.
[32] L. Bucci, M.R. Lavagna, Analytical formulation for light and fast low-thrust guidance design to perform multi-target on-orbit servicing, in: Proceedings of the AIAA Guidance, Navigation, and Control Conference, California, San Diego, 2016, https://doi.org/10.2514/6.2016-0877.
[33] F. Mier-Hicks, P.C. Lozano, Electrospray thrusters as precise attitude control actuators for small satellites, J. Guid. Contr. Dynam. 40 (3) (2017) 642–649, https://doi.org/10.2514/1.G000736.